SAND2022-5827J

This manuscript was accepted by Rev. Sci.Instrum. Click here to see the version of record.

Coarse spectral characterization of warm x-rays at the Z facility using a filtered thermoluminescent dosimeter array

V. J. Harper-Slaboszewicz [a)], B. A. Ulmen, C. T. Parzyck[b)], D. J. Ampleford, A. L. McCourt, K. S. Bell, and C. A. Coverdale

Sandia National Laboratories, P. O. Box 5800, Albuquerque, New Mexico 87185-1159 USA

A new collimated filtered thermoluminescent dosimeter (TLD) array has been developed at the Z facility to characterize warm x-rays ($h\nu > 10$ keV) produced by Z pinch radiation sources. This array includes a Kapton debris shield assembly to protect the TLDs from the source debris, a collimator array to limit the field of view of the TLDs to the source region, a filter wheel containing filters of aluminum, copper and tungsten up to 3 mm thick to independently filter each TLD, and a hermetically-sealed cassette containing the TLDs as well as tungsten shielding on the sides and back of the array to minimize scattered radiation reaching the TLDs. Experimental results from a krypton gas puff and silver wire array shot are analyzed using two different functional forms of the energy spectrum to demonstrate the ability of this diagnostic to consistently extend the upper end of the x-ray spectrum characterization from ~ 50 keV to greater than 1 MeV.

I. INTRODUCTION

The Z pulsed power facility[1] has the capability of deploying several types of loads that provide high fluences of warm x-rays such as gas puffs[2] and Z-pinch wire arrays[3]. These sources radiate strongly in the energy range 1–10 keV, and Z has a suite of diagnostics very well suited to diagnosing the spatial, spectral and temporal characteristics of x-rays up to 15 keV. However, these diagnostics are less suitable at higher energies. The end of the spectral range of the highest photon energy spectrometer is 20–25 keV[4], and diamond photoconducting detector absorption drops below 5% at higher energy[5]. In addition, these diagnostics are not calibrated for higher photon energies.

More recently, increased attention to x-rays with energies above 10 keV has been motivated by the development of non-thermal sources designed to produce radiation in this spectral region. In addition, the continuum in this higher range from sources producing lines below 10 keV can affect experiments using those line sources, so it is useful to better characterize that continuum. New diagnostics specifically designed for the energy range above 20

[a)] Author to whom correspondence should be addressed. Electronic mail: vjharpe@sandia.gov

[b)] This research was performed while C. T. Parzyck was at Sandia National Laboratories, P. O. Box 5800, Albuquerque, New Mexico 87185-1159

keV are being developed to allow characterization of the x-ray environment, as well as to allow assessment of the relevant load physics. The diagnostics include a differentially-filtered time-integrated pinhole camera[6], a differentially-filtered time-resolved x-ray spectrometer[7], and a bent-crystal spectrometer designed to cover the 6.7–86 keV range using interchangeable crystals[8].

Taking advantage of the existing calibration infrastructure for thermoluminescent dosimeters (TLDs), the differentially-filtered TLD array determines the x-ray energy in a filter channel to provide a calibrated measure of yield in that channel. Measurements of the high energy portion of the x-ray energy produced at the Z facility using differentially filtered TLDs have been reported previously[9,10]. While the previous results used a diagnostic primarily sensitive to spectral differences in the range $h\nu$ = 100–2000 keV[11], the diagnostic and results presented here focus on the energy range $h\nu$ = 10–100 keV. Although the intent is to use the data provided by this array in conjunction with other spectral diagnostics, this paper will focus on the data provided by this array in isolation.

This diagnostic provides a coarse but calibrated constraint on the spectral energy content at high energy produced by warm x-ray sources on the Z facility. First the physical design and the spectral response of the chosen filters are discussed. Experiments to determine the spatial uniformity of the measurement by flat field shots are shown. The data for two types of Z warm x-ray sources are presented and analyzed by fitting to two different models of the spectral distribution. The paper concludes by examining the spectral energy content in selected energy bins for these x-ray sources.

II. DIFFERENTIALLY-FILTERED TLD ARRAY DESIGN

Mn-doped calcium fluoride thermoluminescent dosimeters (TLD-400)[12] were chosen as the dose recording medium. They have high sensitivity and linear response over a broad range of energy depositions, recording energy depositions from 1 μJ/g (1mGy) to 1 J/g (1 kGy), and have enhanced response in the energy range 10–200 keV due to the photoelectric response of the calcium. In addition, this choice leverages the NIST-traceable calibration of the TLD reading system established at Sandia National Laboratories Radiation Metrology Laboratory to provide absolute measurements of warm x-ray energy deposition[13].

Z-pinch radiation sources on the Z facility produce an intense debris environment including a strong ultraviolet radiation pulse, a thermal and pressure pulse from expanding vaporized source region materials, and solid particles from disassembling materials near the source region. A Kapton debris shield assembly, with a total material thickness of 0.45 mm, is mounted on the front of the TLD array to protect the array from debris and to maintain the integrity of the hermetic seal. Because the center section of the Z facility is a beryllium contaminated environment, the hermetic seal ensures that no debris enters the housing and thus the TLDs can be recovered and read. This debris shield assembly limits the photon energies incident on the TLDs to >5 keV.

The first element of the diagnostic shown in Figure 1 is the debris shield assembly. This is followed by a collimator, 2.15 cm thick, with ten parallel cylindrical apertures, each 0.5 cm in diameter. The collimator restricts the field of view of the diagnostic to the region near the source, blocking scattered radiation and bremsstrahlung from electron losses in the magnetically insulated transmission lines and post-hole convolute. One aperture is located on the centerline of the assembly and the remaining nine are equally spaced with centers on a circle of radius 1.78 cm. Behind the collimator is a filter wheel which can accommodate filters up to 3 mm thick. Next is the TLD housing holding 10 bare CaF_2:Mn TLDs (TLD-400) 3.2 mm square and 0.9 mm thick, with a 0.25 mm aluminum cover plate acting as an equilibrator. Equilibration ensures that the absorbed dose is directly related to the photon fluence by creating a secondary electron flux into the detector which balances the secondary electron flux out of the detector, since photon energy is deposited by creating secondary electrons[14]. This equilibrator limits the photon energies incident on the TLDs to >8 keV. A 7 mm thick tungsten back plate blocks backscattered radiation from the center section wall from the TLDs. Scattered radiation from the vicinity of the source is limited by the collimator. The solid angle viewed by the TLDs between the collimator and the back plate is relatively small, so no additional radiation shielding is provided for scattered radiation entering the diagnostic from the side. The entire assembly is encased in a hermetically-sealed housing with an external dimension of 5 cm wide by 5 cm tall by 4.35 cm deep. This compact housing and simple design allows for ease of installation and the ability to be fielded underneath the traditional 12 degree line of sight on Z, meaning it can be fielded on the same sight line as other diagnostics. This increases the flexibility in choosing where and when to field.

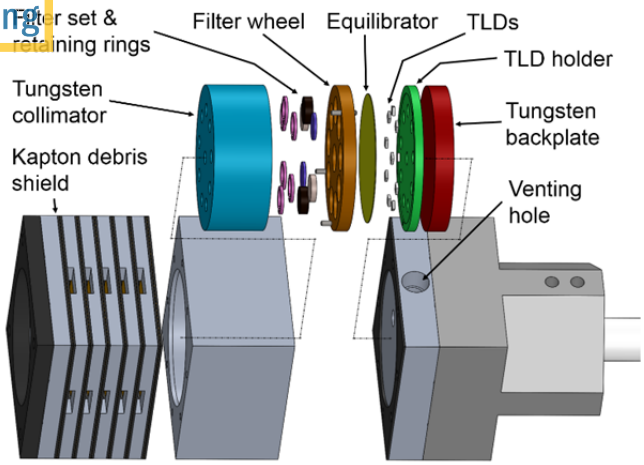

FIG. 1. Exploded view of TLD array inside the housing.

The collimating apertures limit the fields of view of the TLDs. At a fielding distance of 88 cm, the field of view of each of the TLDs is approximately a disk of radius 4 cm at the source plane. Since nominal radiation sources on the Z facility are vertical cylinders about 2 cm tall and 0.5 cm in diameter, the source is fully within the field of view of all of the TLDs when the centerline of the array is aligned with the center of the source.

Different filter sets may be selected to meet spectral sensitivity and resolution requirements of different experiments. All TLDs were filtered by the Kapton debris shield assembly and the thin aluminum equilibrator. The filter set used to collect the data presented in this paper included nine different filters, consisting of 1.0, 2.0, and 3.0 mm thick disks of aluminum (Al1, Al2, Al3), copper (Cu1, Cu2, Cu3), and tungsten (W1, W2, W3). Additionally, one TLD had no additional filtering (Open). This set of filters was selected to provide sensitivity in response to warm x-ray energies. The response functions for this filter set, including the effect of the debris shield assembly were calculated using the discrete ordinates code CEPXS[15], and are shown in Figure 2. The cutoff at about 8 keV is due to the aluminum equilibrator, and the peak in response between 10 and 200 keV is characteristic of calcium fluoride. The source of the separation of the responses above 1 MeV is that the equilibrator is too thin to create a balanced flux of secondary electrons at these high energies.

This manuscript was accepted by Rev. Sci.Instrum. Click here to see the version of record.

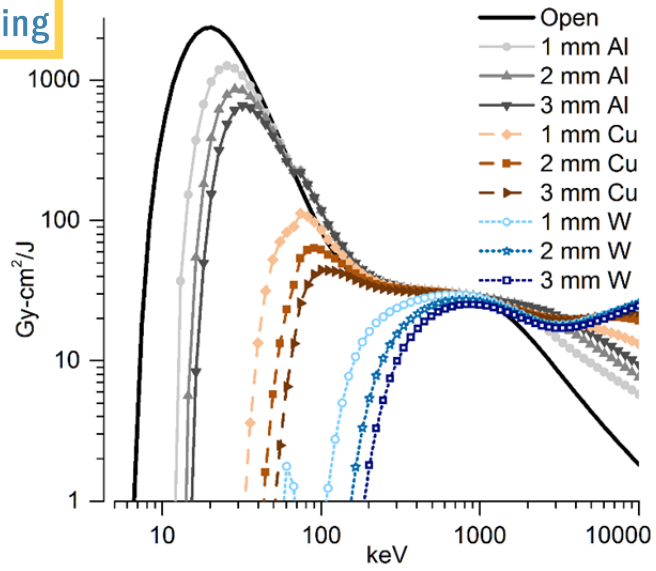

FIG. 2. Dose response functions for TLD assembly behind the selected filter set. The response functions include the filtering due to the debris shielding (0.45 mm Kapton) and the equilibrator (0.25 mm aluminum) in front of each of the TLDs. The units are dose per unit energy fluence.

III. EXPERIMENTAL RESULTS

A. Flat field response

Interpretation of the results from this diagnostic depends on calculating the differential response between TLDs with different filters at different locations within the diagnostic. It is therefore important to characterize the response of unfiltered TLDs in different azimuthal locations to verify that there is no important difference in response between different locations. The flat field shot provides this verification. The results are shown in Figure 3. For this shot, all of TLDs were filtered only by the equilibrator and Kapton debris shield assembly. The error bars show the quoted 1-σ uncertainties in the dose, which include approximately equal amounts of Type A and Type B uncertainty[16]. Type A uncertainty is evaluated using the statistical analysis of a series of observations, and is broadly similar to aleatoric uncertainty, while Type B uncertainty is evaluated using other methods, and is broadly similar to epistemic uncertainty. The results are consistent with the all of the TLDs viewing the same source, with the dose variation accounted for by the uncertainty in the TLD response.

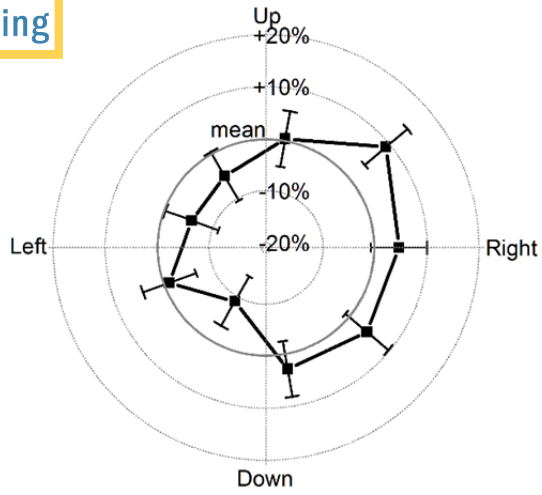

FIG. 3 – Percentage difference in angular position dose relative to mean dose for flat field shot (empty filter wheel) at 90 cm from source.

B. Shot data

The data analyzed using this diagnostic come from five different shots: two krypton gas puff sources and three wire array sources (two silver wire arrays and one molybdenum wire array). The diagnostic was fielded at 82 cm for all shots to minimize the effect of misalignment. The measured doses along with the measurement uncertainty are shown in Table I.

TABLE I. CaF_2:Mn TLD measurements and total uncertainty.

	Z_2533 Mo wire array		Z_2534 Ag wire array		Z_2535 Ag wire array		Z_2542 Kr gas puff		Z_2543 Kr gas puff	
Filter Type	Dose (Gy)	%unc[a]	Dose (Gy)	%unc[a]	Dose (Gy)	%unc[a]	Dose (Gy)	%unc[a]	Dose (Gy)	%unc[a]
1 mm Al	5.383	4.98	6.783	4.88	5.584	4.96	1.362	5.16	2.263	5.49
2 mm Al	3.939	5.47	4.230	5.08	4.255	5.61	0.7326	5.46	1.054	5.15
3 mm Al	3.616	5.53	3.593	5.53	3.191	5.48	0.6483	5.08	0.8214	5.48
1 mm Cu	1.447	5.47	1.341	5.50	1.405	5.09	0.2590	5.22	0.2819	5.20
2 mm Cu	1.544	5.44	1.301	5.51	1.347	5.62	0.2162	5.27	0.2030	5.29
3 mm Cu	1.121	5.56	1.249	5.64	1.236	5.49	0.2013	5.29	0.2326	5.25
1 mm W	0.8868	5.62	0.8202	5.63	0.9947	5.60	0.1669	4.57	0.1778	4.54
2 mm W	0.9617	5.62	0.7927	5.64	0.9717	5.64	0.1130	4.88	0.1118	4.89
3 mm W	0.8401	5.63	0.8034	5.64	0.7836	5.53	0.1145	4.87	0.1099	4.91
Open	18.67	5.11	15.01	5.07	12.92	5.05	6.783	5.52	16.70	5.52

[a]total uncertainty including type A and type B

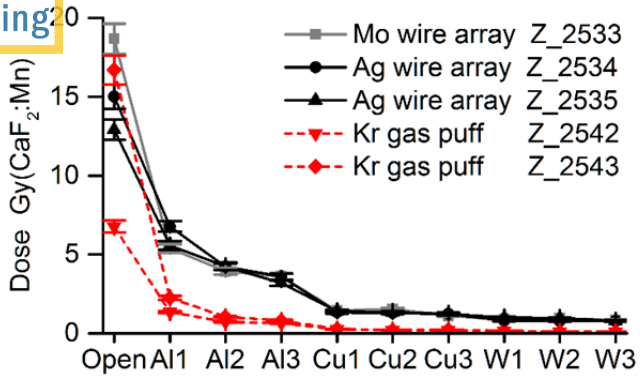

FIG 4. TLD doses measured on 5 shots (Table I). All TLDs were filtered by the Kapton debris shield and the aluminum equilibrator. Al1, Al2, Al3, etc. correspond to the filter material and thickness in mm. The Kr gas puff sources (red, dashed) always show lower doses than the wire arrays for the highly filtered TLDs.

The three wire array shots have similar dose profiles. On the two gas puff shots, the TLDs filtered by copper and tungsten record similar doses, but there is a significant difference in the doses to the unfiltered and aluminum filtered TLDs. Inspection of the response functions in Figure 2 suggests that this reflects a difference in the x-ray energy spectrum below about 30 keV. On the wire array shots, the more highly filtered TLDs, behind the tungsten filters, record about eight times more dose than the similarly filtered TLDs on the gas puff shots. Inspection of the response functions suggests that this reflects a difference in the x-ray energy spectrum above about 100 keV. These differences show that this diagnostic is sensitive to differences in the x-ray energy distribution between different sources. This paper will focus on the analysis of one wire array shot (Z_2534) and one gas puff shot (Z_2543) to illustrate this capability.

IV. ANALYSIS OF EXPERIMENTAL RESULTS

The x-ray energy range to which this diagnostic responds, from 8 keV to greater than 1000 keV, encompasses both the high energy tail of continuum radiation from the hot z-pinch plasma and bremsstrahlung from very energetic electrons. This bremsstrahlung originates primarily in the vicinity of the pinch[9]. The timing of this energetic radiation, which arrives about 10 ns after the peak of the soft x-ray pulse[7], supports the idea that it results from energetic electrons striking the source hardware after the disassembly of the z-pinch. Although the resolution of this diagnostic is coarse, it can provide bounds on the x-ray fluence at these higher energies, to which many of the other diagnostics on Z are not sensitive. Determination of the fluence requires characterization of the

spectrum. Unfolding techniques which do not require a priori assumptions of the spectral shape, such as the Backus-Gilbert method, have been successfully used in other x-ray diagnostic settings[17-22]. Similar analysis was conducted for data collected from this diagnostic, but the coarseness of the spectral information resulted in unphysical results. As a result, this approach was abandoned in favor of a constrained unfolding method based on simple physical models of the spectral shape.

Two simplified physical models were selected to fit the data and provide an energy estimate. The first model assumes the spectrum is composed of a low temperature thermal plasma bremsstrahlung along with an attenuated bremsstrahlung spectrum and a single K-shell line. The low temperature component provides a characterization of the tail of the thermal radiation output of the z-pinch plasma. Although it neglects opacity effects and details of the atomic interactions, it is a plausible model for thermal tail. The second term represents the physical process by which these very high energy photons are produced, which is believed to be bremsstrahlung from an energetic electron beam (up to 6 MeV) striking the anode after disassembly of the Z pinch, as viewed by this diagnostic. The line component accounts for energy in the line for which the source was designed.

The second model is a two-temperature thermal plasma bremsstrahlung model with a single K-shell line. The low temperature thermal component and single line component are identical to the first model. The high temperature thermal component, although less physically plausible, provides a smooth fit which drops off rapidly at high energies. It is intended to provide an estimate of the energy above the thermal low energy tail. This model differs from the thermal + attenuated model in two ways. First, it declines exponentially rather than going to zero at the beam electron energy. Second, the high temperature thermal component contributes to the low energy spectrum, rather than being cut off at low energy by absorption of the x-rays in the material filtering the bremsstrahlung. In both cases, the spectrum produced by the thermal components is modeled as thermal bremsstrahlung. These simplified models do not fully represent the photon energy spectrum, but provide a simplified parameterization with resolution appropriate for the resolution of the diagnostic.

This manuscript was accepted by Rev. Sci.Instrum. Click here to see the version of record.

Although the analysis is not shown here, it should be noted that no single component model was able to fit both the lightly filtered TLD and the strongly filtered TLD data. A two-component model was required to fit all of the data.

A. Parametric spectral models

The differential photon number spectrum, ψ, incident on the detector is assumed to be of one of the two following forms:

$$\psi(E) = A\exp(-E/T_1) + B\left(\frac{E_{end}}{E} - 1\right)^{1.55}\Theta(E_{end} - E)\exp(-Q\mu(E)) + L\delta(E - E_l) \quad (1)$$

$$\psi(E) = A\exp(-E/T_1) + B\exp(-E/T_2) + L\delta(E - E_l) \quad (2)$$

Equation 1 describes the first model, thermal + attenuated bremsstrahlung, where the first term is the low temperature thermal bremsstrahlung term, the second term is a modified Kramer's law[22] term filtered by a material thickness Q, and the third term is the line spectrum; Θ is the Heaviside step function and δ is the Dirac delta. The modified[23] Kramer's law has an exponent 1.55 chosen for this application to account for the reduction in high energy photons in the bremsstrahlung spectrum at angles away from the forward direction. The exponent was calculated based on the backscattered bremsstrahlung spectrum from an intense electron beam normally incident on a thick material, measured at a nearly grazing angle to the material surface. This approximates the geometry of the electron beam striking the anode after disassembly of the pinch, as viewed from this diagnostic. The free parameters are A, B, T_1, Q, and L; $\mu(E)$ is the energy-dependent mass attenuation factor for stainless steel from the NIST x-ray attenuation database. E_{end} is held fixed for each shot analysis at 6000 keV, considered to be the peak voltage on the Z facility and thus the maximum energy of the post-pinch electron beam.

Equation 2 describes the two temperature thermal bremsstrahlung model where the first two terms are the low energy and high energy thermal bremsstrahlung terms, and the third term is the line spectrum. In this model A, B, T_1, T_2, and L are the free parameters. In both models the x-ray line energy, E_l, is held fixed at 13 keV for the krypton K-shell line or at 22 keV for silver.

This manuscript was accepted by Rev. Sci.Instrum. Click here to see the version of record.

Both of these equations fit the time- and spatially-integrated data to a simplified single point representation of the radiation source characteristics, so the fitted parameters are expected to be in only coarse agreement with the more detailed representations of the radiation source.

B. Parametric spectral unfold method

The set of response functions, $R_i(E), i = 1,\ldots,M$, for the various channels shown in Figure 2 relate the number spectrum, ψ, to the channel doses, D_i, by a simple integral folding

$$D_i = \int_0^{10MeV} \psi(E) R_i(E) dE \approx \sum_{j=1}^{N} \psi(E_j) R_i(E_j) \Delta E_j \qquad (3)$$

The calculation was bounded at 10000 keV, above the 6000 keV E_{end} to allow the two temperature thermal model to vary its high energy tail. Since the number of channels ($M = 10$) is much smaller than the number of sample points used in the estimation of the integral (N ~ 200) the inverse problem of extracting ψ from a set of experimentally measured TLD dose data, $D_i^{\exp}, i = 1,\ldots,10$ is ill-posed. Instead, a minimizer of the objective function

$$f(x) = \sum_{i=1}^{10} \left(1 - \frac{1}{D_i^{\exp}} \int_0^{\infty} \psi(E; x) R_i(E) dE \right)^2 \qquad (4)$$

is sought. Here, x is a vector of non-negative parameters: $x = (A, B, T_1, Q, L)$ for the thermal + attenuated bremsstrahlung model and $x = (A, B, T_1, T_2, L)$ for the two temperature thermal bremsstrahlung model. The dose term in the denominator explicitly makes the objective function equally sensitive to the all of the measured doses, which vary over two orders of magnitude. Because the uncertainty in the TLD reading is an approximately constant fraction of dose, as seen in Table I, this form of the objective function is equivalent to one using the reciprocal of the variance as the weighting function. This minimization problem can be solved using an iterative method given a reasonable starting estimate of the parameters. A comparison of two minimization algorithms, Nelder-Mead[24], which is a simplex method, and Levenberg-Marquardt[25,26], which is a hybrid Gauss-Newton and gradient descent

This manuscript was accepted by Rev. Sci.Instrum. Click here to see the version of record.

method, showed that the latter produced a smaller variation in the final fit with less likelihood of a bimodal parameter distribution and was thus used in the presented analysis.

C. Monte Carlo uncertainty quantification method

In addition to the experimentally measured dose, $D_i^{\exp}$, the uncertainty in that measurement, $\delta D_i^{\exp}$, is also known. To investigate how this uncertainty affects the parameters of best fit a series of trials were run. In each trial a set of perturbed does, $D_i^{per}, i = 1,\ldots M$ were selected from a normal distribution with mean $D_i^{\exp}$ and standard deviation $\delta D_i^{\exp}$. The vector of parameters x, which minimizes the objective function,

$$\sum_{i=1}^{M}\left(1-\frac{1}{D_i^{per}}\int_0^{\infty}\psi(E;x)R_i(E)dE\right)^2 \tag{5}$$

was then computed and the results were tallied for 2000 such trials (the starting parameters, x_0, are held fixed for all trials). The fitting results were found to be insensitive to the choice of x_0. The choice of 2000 trials assured multiple sampling of the tails of the distributions of the doses while still resulting in reasonable computational times.

D. Parametric unfold results

The spectra resulting from fitting the two models to the gas puff and wire array sources are shown in Figure 5. Only the portion above 8 keV is plotted because this diagnostic provides no information for x-ray energies below this energy due to filtering by the debris shielding and equilibrator. The resulting spectra show significant differences.

Consider first the high energy portion of the spectra, above about 50 keV. Although the shapes of the spectra produced by the thermal + attenuated model, in the top of the figure, and the two temperature model, in the bottom of the figure, differ somewhat, the amplitudes and general shapes agree well. The differences between the two models are largest at low energy, below about 50 keV. For the Kr gas puff, on the left of the figure, the low energy continuum from the two temperature thermal fit is two orders of magnitude higher than for the thermal + attenuated

This manuscript was accepted by Rev. Sci.Instrum. Click here to see the version of record.

fit. For the wire array, on the right of the figure, the resulting spectra look similar at the low energy range. Note that in all cases the fitted spectrum includes both a high energy and a low energy component.

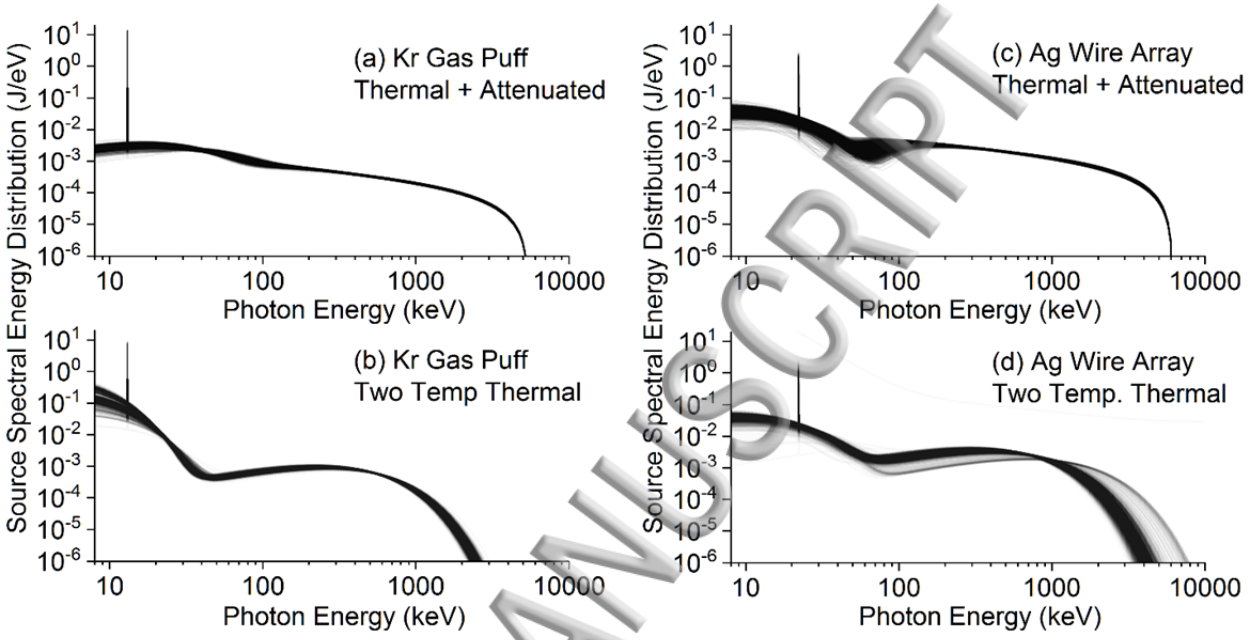

FIG 5. Fitted source energy spectrum for the two types of spectral fits for the (a-b.) Kr gas puff source and the (c-d.) Ag wire array created by overlapping 2000 Monte Carlo trials in which the TLD data were varied using the known variance and the resulting data were fitted using the two source models. For the Kr Gas Puff source, the line feature at 13 keV is the K-shell emission of the Kr source. For the Ag Wire Array the line feature at 22 keV is the K-shell emission of the Ag source.

The relationship of these modeled spectra to the individual TLDs in the diagnostic is illustrated in Figure 6. The contribution of each spectral component to the dose in each TLD is shown for the wire array and the gas puff for both models. The two graphs in the left column show the dose in each TLD from each component, while the center and right column graphs show the fraction of the dose in each TLD from each component. The dose in the copper and tungsten filtered TLDs comes almost entirely from the high temperature thermal or attenuated bremsstrahlung component. Examining the dose in the open TLD, the wire array shows little difference in the percentage of energy in the low energy, high energy, and line components while there is a significant difference in these percentages for the gas puff. The open and lightly filtered Al1 doses in the gas puff show significant trade-off in the two models between the dose in the line and the dose in the low temperature thermal bremsstrahlung. Because the krypton K-

and line occurs at lower energy than the silver line, this means that the diagnostic cannot effectively resolve the difference between a strong line and a strong continuum at energies below about 20 keV.

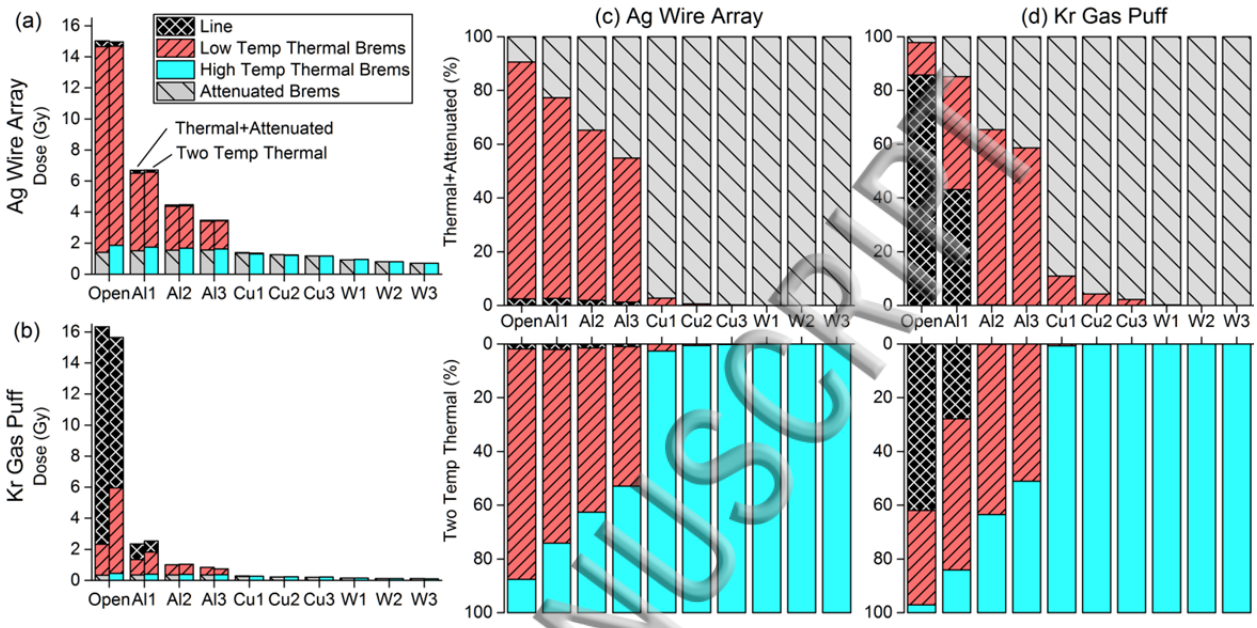

FIG 6. (a-b.) Breakdown of dose and (c-d.) percentage of deposited dose of the spectral components for each TLD filter for the Ag wire array and Kr gas puff.

E. Monte Carlo uncertainty quantification

Histograms of the distribution of fitted parameter values resulting from the Monte Carlo variation of the TLD dose are shown in Figures 7 and 8 for the gas puff and wire array shots.

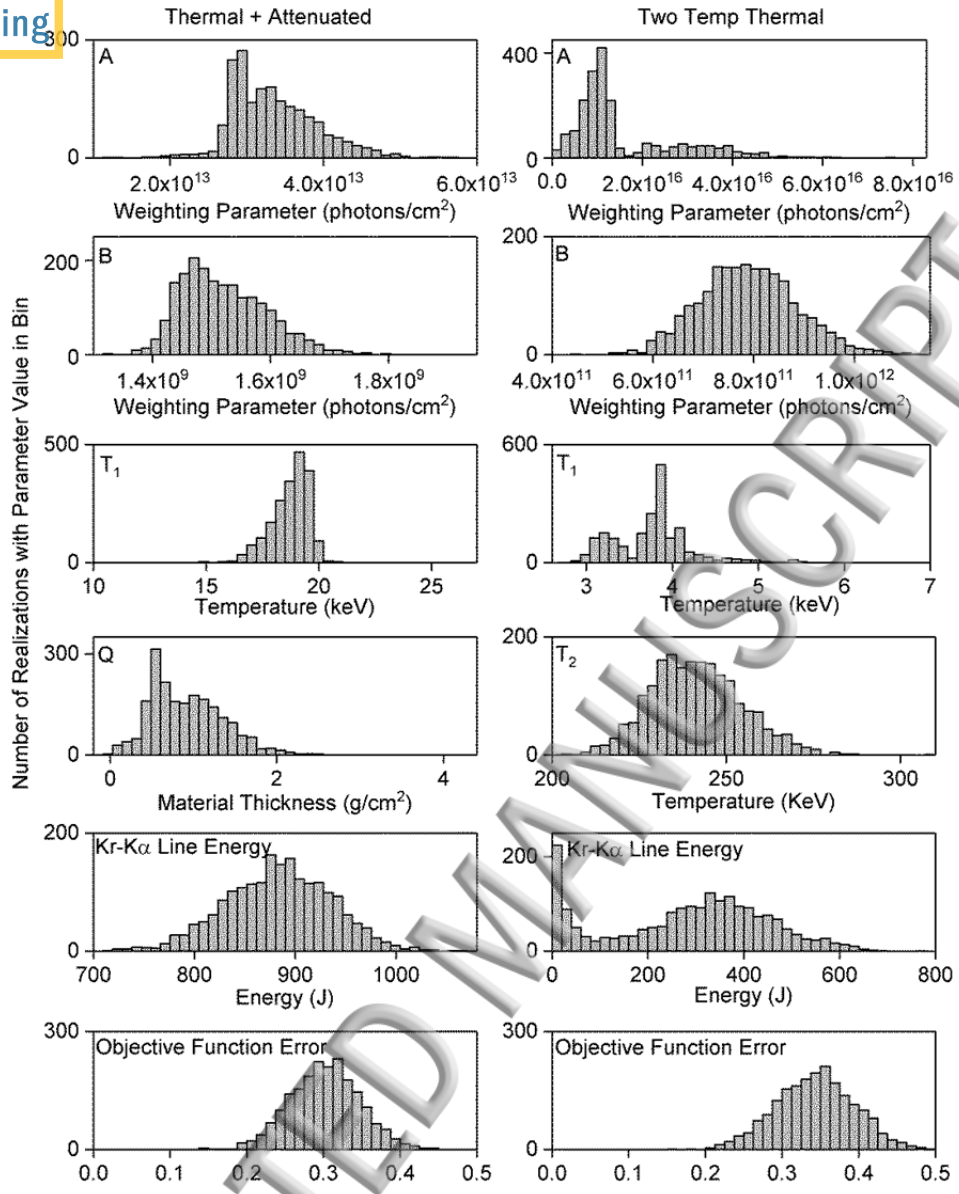

FIG 7. Histograms of parameter space found in the Monte Carlo uncertainty quantification for the two functional forms for shot Z_2543 Kr gas puff source. In each subplot, the y-axis is the number of realizations out of 2000 resulting in the parameter value in the bin, and the x-axis is the parameter value. *A* is the amplitude of the low energy thermal term, *B* is the amplitude of the high energy thermal or bremsstrahlung term, T_1 is the low temperature, T_2 is the high temperature, *Q* is the effective material thickness filtering the bremsstrahlung, and the error term is the objective function defined in equation 5.

The distribution of the parameters which characterize the high energy photon spectrum, *B* or T_2, for both models for the gas puff shot is relatively narrow, with a half-width of 10% or less, as seen in Figure 7. By contrast, the

This manuscript was accepted by Rev. Sci.Instrum. Click here to see the version of record.

distributions of the parameters which characterize the low energy portion of the spectrum, A, T_1, Q, and line energy, are broader. This is likely because the high energy portion of the spectrum is defined by only two parameters, while determining the dose to six of the TLDs. On the other hand, the low energy portion of the spectrum is influenced by all five parameters, while strongly affecting the dose to only four TLDs. This means that the fit of the low energy portion of the spectrum is more weakly constrained.

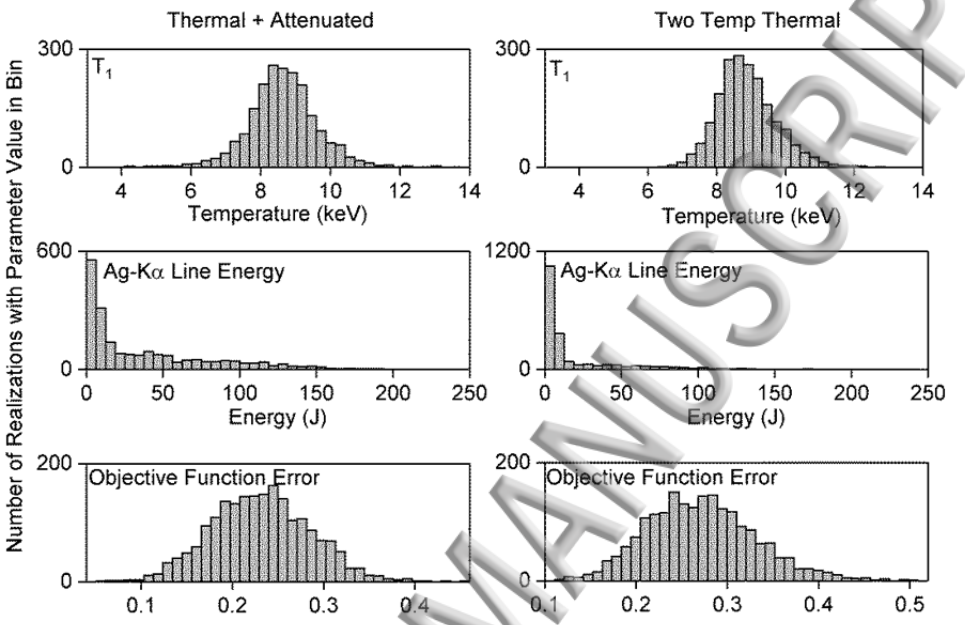

FIG 8. Histograms of parameters found in the Monte Carlo uncertainty quantification for shot Z_2534 Ag wire array comparing the low temperature thermal bremsstrahlung and line energy components, as well as the error term, which is the objective function defined in equation 5. In each subplot, the y-axis is the number of realizations out of 2000 resulting in the parameter value in the bin, and the x-axis is the parameter value.

The distribution of the parameters which characterize the photon spectrum for both models for the wire array shot is relatively narrow, with a half-width of 10% or less, with the exception of the line energy, as seen in Figure 8. For this source the filter set appears to provide sufficient information to constrain the spectrum, except that it lacks the resolution to pick out the line from the low energy spectrum.

F. Energy in bands

These fitted spectra can be used to compute the x-ray energy in various ranges. Figure 9 shows the results of these calculations. The bulk of the warm (10–100 keV) and hot (>100 keV) x-ray energy produced by the wire array

is in the hot x-ray energy range, with 3.1–3.4 kJ in the hot x-ray band. By contrast, the bulk of the warm and hot x-ray energy produced by the gas puff is in the warm x-ray band, with about 0.9–1.1 kJ in the warm x-ray band. For both shots, the two temperature thermal spectral model results in a total energy about 10% higher than the thermal + attenuated model. The reason for this systematic difference is not clear. However, the agreement between the calculated energies using two different physical models to fit the spectrum suggests that this diagnostic provides a robust measurement of the energy in broad bands of the warm and hot x-ray spectrum, with an error of order 10%.

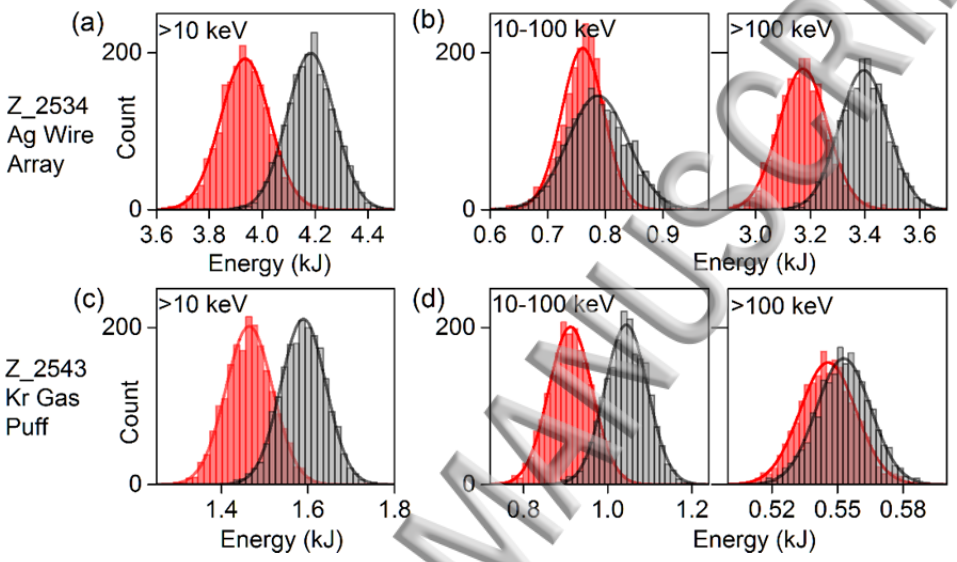

FIG 9. Results of the Monte Carlo evaluation of uncertainty shown as histograms of the total energy above 10 keV, the energy in the bin 10-100 keV, and the energy >100 keV for the Ag wire array and Kr gas puff sources. The red distribution shows the results for the Thermal + Attenuated Bremsstrahlung model, and the grey distribution shows the results for the Two Temperature Thermal Bremsstrahlung model.

It should be noted that the best fits produced by this procedure still have a large residual error in the fitted dose. The expected value of the objective function is 0.16, with a standard deviation of 0.02, using the uncertainties in Table I, while the values of the objective function from the fits to the Monte Carlo data are centered between 0.2 and 0.35. This confirms that these very simplified models are incomplete representations of the spectral energy distributions from these sources.

V. CONCLUSION

The differentially filtered TLD array described here provides a characterization of the warm and hot x-ray spectrum produced by x-ray sources on the Z facility and insight into mechanisms producing emissions up to 10000 keV. The experimental data is fit reasonably well by two physical models with a small number of free parameters: a low temperature thermal plasma bremsstrahlung with an attenuated high energy electron bremsstrahlung and a two temperature thermal plasma bremsstrahlung. The five parameters of each of these models were fit using a Levenberg-Marquardt minimization with a Monte Carlo simulation of the parameter space used to explore the uncertainty in the fit. The fits were reasonable for both models for both the krypton gas puff source and the non-thermal wire array, however it was found that this diagnostic cannot distinguish the low temperature thermal plasma bremsstrahlung background from the line radiation, resulting in greater uncertainty in the fit at the low energy range. Reasonable fits to the TLD data are obtained only when both the low energy and high energy terms contribute substantially to the measured energy deposition. This diagnostic allows characterization of both the low energy and high energy terms using sensors with the same field of view, response characteristics, and calibration basis.

This diagnostic produces a robust, absolutely calibrated, though coarse measurement of the energy fluence in the range 10–10000 keV from z-pinch radiators on Z. The two sources examined, the Kr gas puff and Ag wire array differ widely in their K shell emission mechanism and this diagnostic provides the capability to examine the spectral content of both sources.

ACKNOWLEGEMENTS

The authors would like to thank the program leadership team of Patrick J. Griffin and Michael E. Cuneo for their support of this work. The authors acknowledge useful discussions on issues of data analysis with David Fehl and Robert Hohlfelder. Excellent support for the experiments reported here was provided by the staff of the Z facility and the Radiation Metrology Laboratory. This work was supported by the Laboratory Directed Research and Development program at Sandia National Laboratories, a multi-mission laboratory managed and operated by Sandia Corporation, a wholly owned subsidiary of Lockheed Martin Corporation, for the U.S. Department of Energy's National Nuclear Security Administration under contract DE-AC04-94AL85000.

REFERENCES

[1]M. E. Savage, K. R. LeChien, M. R. Lopez, B. S. Stoltzfus, W. A. Stygar, D. S. Artery, J. A. Lott, and P. A. Corcoran, in *Proceedings of the 18th IEEE International Pulsed Power Conference*, Chicago, USA, 19 June-23 June 2011, (IEEE Press, Piscataway, NJ, 2011) pp. 983-990.

[2]B. Jones, C. A. Jennings, D. C. Lamppa, S. B. Hansen, A. J. Harvey-Thompson, D. J. Ampleford, M. E. Cuneo, T. Strizic, D. Johnson, M. C. Jones, N. W. Moore, T. M. Flanagan, J. L. McKenney, E. M. Waisman, C. A. Coverdale, M. Krishnan, P. L. Coleman, K. W. Elliot, R. E. Madden, J. Thompson, A. Bixler, J. W. Thornhill, J. L. Giuliani, Y. K. Chong, A. L. Velikovich, A. Dasgupta, and J. P. Apruzese, IEEE Trans. Plasma Sci., 42, 1145 (2014).

[3]D. J. Ampleford, B. Jones, C. A. Jennings, S. B. Hansen, M. E. Cuneo, A. J. Harvey-Thompson, G. A. Rochau, C. A. Coverdale, A. R. Laspe, T. M. Flanagan, N. W. Moore, D. B. Sinars, D. C. Lamppa, E. C. Harding, J. W. Thornhill, J. L. Giuliani, Y.-K. Chong, J. P. Apruzese, A. L. Velikovich, A. Dasgupta, N. Ouart, W. A. Sygar, M. E. Savage, J. K. Moore, R. Focia, T. C. Wagoner, K. L. Killebrew, A. D. Edens, G. S. Dunham, M. C. Jones, P. W. Lake, D. S. Nielsen, M. Wu, A. L. Carlson, M. D. Kernaghan, C. R. Ball, R. D. Scharberg, T. D. Mulville, E. W. Breden, C. S. Speas, G. Olivas, M. A. Sullivan, A. J. York, D. W. Justus, J. C. Cisneros, T. Strizic, J. Reneker, M. Cleveland, M. P. Vigil, G. Robertson, D. Sandoval, C. Cox, A. J. Maurer, D. A. Graham, N. B. Huynh, S. Toledo, L. P. Molina, M. R. Lopez, F. W. Long, G. R. McKee, J. L. Porter and M. C. Herrmann, Phys. Plasmas 21, 056708 (2014).

[4]D. B. Sinars, D. F. Wenger, S. A. Pikuz, B. Jones, M. Geissel, S. B. Hansen, C. A. Coverdale, D. J. Ampleford, M. E. Cuneo, L. A. McPherson, G. A. Rochau, Rev. Sci. Instrum. 82, 063113 (2011).

[5]R. B. Spielman, Rev. Sci. Instrum. 66, 867-870 (1995).

[6]L. A. McPherson, C. A. Coverdale, D. J. Ampleford, J. W. Argo, A. C. Owen, and D. M. Jaramillo, Rev. Sci. Instrum. 87, 063502 (2016).

[7]K. S. Bell, C. A. Coverdale, D. Ampleford, J. E. Bailey, G. P. Loisel, V. Harper-Slaboszewicz, J. Schwarz, E. Christner, C. Turner, L. A. McPherson Jr., C. J. Bourdon, M. D. Kernaghan, M. A. Sullivan, C. Kirtley, and M. E. Cuneo, in *Proceedings of the 43rd IEEE International Conference on Plasma Science*, Banff, Canada, 19 June-23 June 2016.

[8]D. J. Ampleford, S. B. Hansen, C. A. Jennings, T. J. Webb, V. Harper-Slaboszewicz, G. P. Loisel, T. M. Flanagan, K. S. Bell, B. Jones, L. A. McPherson, G. A. Rochau, J. P. Chittenden, M. Sherlock, B. Appelbe, J. Giuliani, N. Ouart, J. Seely, SAND2015-10453, Sandia National Laboratories, Albuquerque, NM, December, 2015.

[9]G. E. Rochau, M. Derzon, D. Fehl, G. A. Rochau, M. A. Sweeney, D. Tabor, S. E. Lazier, D. Droemer, T. Helvin and R. Starbird, Rev. Sci. Instrum. 70, 553 (1999).

[10]M. Derzon, T. Nash, G. Chandler, G. Cooper, D. Fehl, C. Hall, J. Lash, R. Leeper, E. McGuire, R. Moch, R. Olsen, C. Olson, G. E. Rochau, G. A. Rochau, C. Ruiz, J. Seamen, S. Slutz, W. Stygar, M. A. Sweeney, S. Lazier, D. Droemer, T. Helvin, and R. Starbird, Rev. Sci. Instrum., 70, 566 (1999).

[11]G. A. Carlson, D. L. Fehl, L. J. Lorence Jr., Nucl. Inst. Meth. B, 62, 264 (1991).

[12]Oliveira, M. L., & Caldas, L. V. Radiation protection dosimetry, 111(1), 17-20, (2004).

[13]ASTM Standard E668, 2013, ASTM International, West Conshohocken, PA, 2003.

[14]F. H. Attix, *Introduction to Radiological Physics and Radiation Dosimetry*. (John Wiley & Sons, 2008) pp. 70–75.

[15]L. J. Lorence, IEEE Trans. Nuc. Sci., 39, 1031 (1992).

[16]JCGM100:208, *Evaluation of measurement data – Guide to the expression of uncertainty in measurement*. (JCGM, 2008) p 6. (http://www.bipm.org/utils/common/documents/jcgm/JCGM_100_2008_E.pdf)

[17]D. L. Fehl, F. Biggs, G. A. Chandler, and W. A. Stygar, Rev. Sci. Instrum. 71, 3072-3079 (2000).

[18]G. E. Backus and J. F. Gilbert, Geophys. J. R. Astron. Soc. 13, 247 (1967).

[19]G. E. Backus and J. F. Gilbert, Geophys. J. R. Astron. Soc. 16, 169 (1968).

[20]G. E. Backus and J. F. Gilbert, Philos. Trans. R. Soc. London 266, 123 (1970).

[21]T. J. Loredo and R. I. Epstein. Astrophys. J., 336, 896 (1989).

[22]H. A. Kramers, Philo. Mag., 46, 836-871 (1923).

[23]N. Broll, and P. de Chateaubourg, in *Advances in X-ray Analysis: Proceedings of the Denver X-ray Conference on Applications of X-ray Analysis*, Denver, USA, 4 August-8 August 1997, (International Centre for Diffraction Data, 1999) 41, pp. 393-402.

[24]J. Nelder and R. Mead, The Computer Journal, 7, 308, (1965).

[25]J. J. Moré, *The Levenberg-Marquardt algorithm: implementation and theory* (Springer, Berlin, 1978).

[26]R. Fletcher, *A modified Marquardt subroutine for non-linear least squares* (Atomic Energy Research Establishment, United Kingdom, 1971).

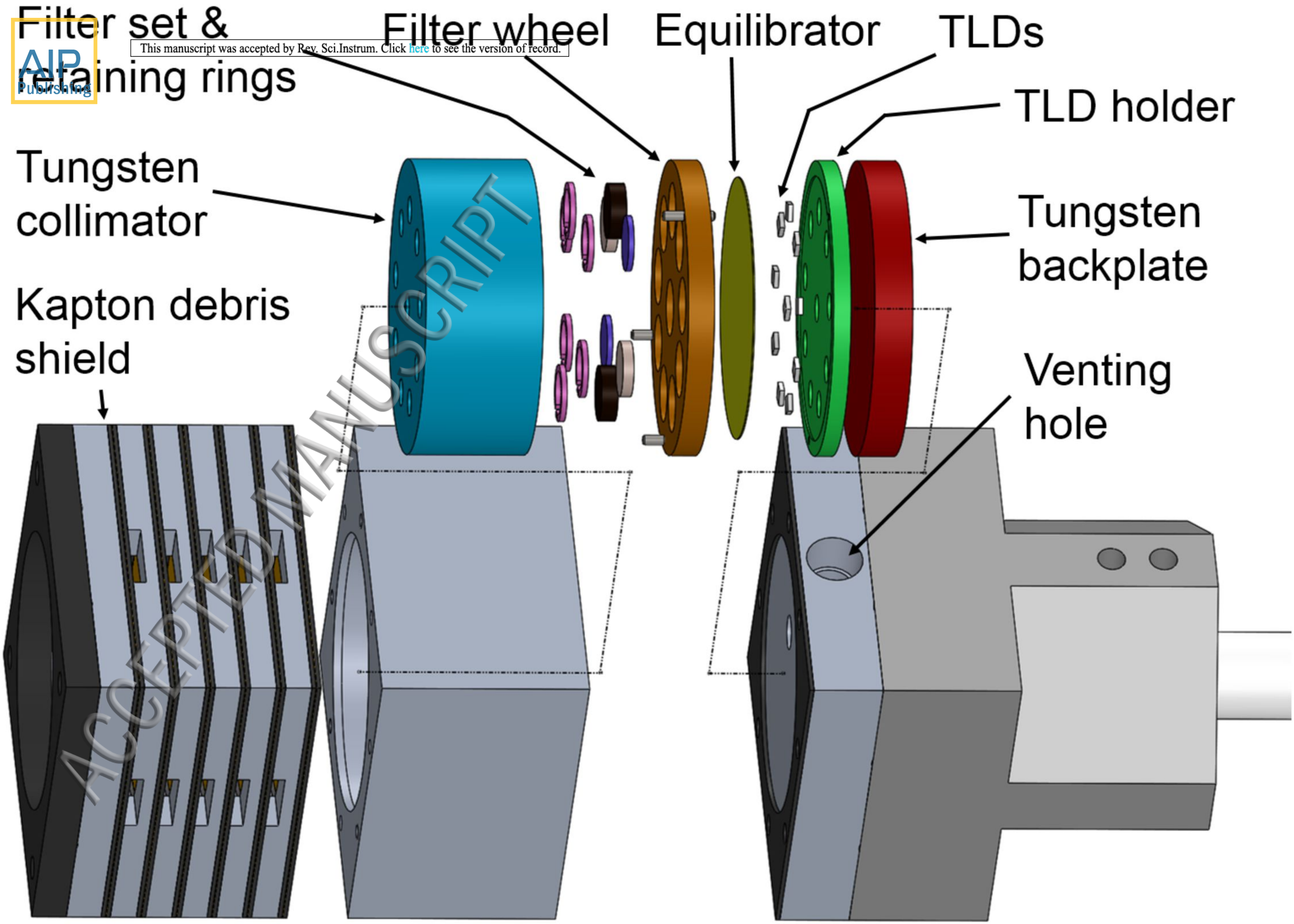

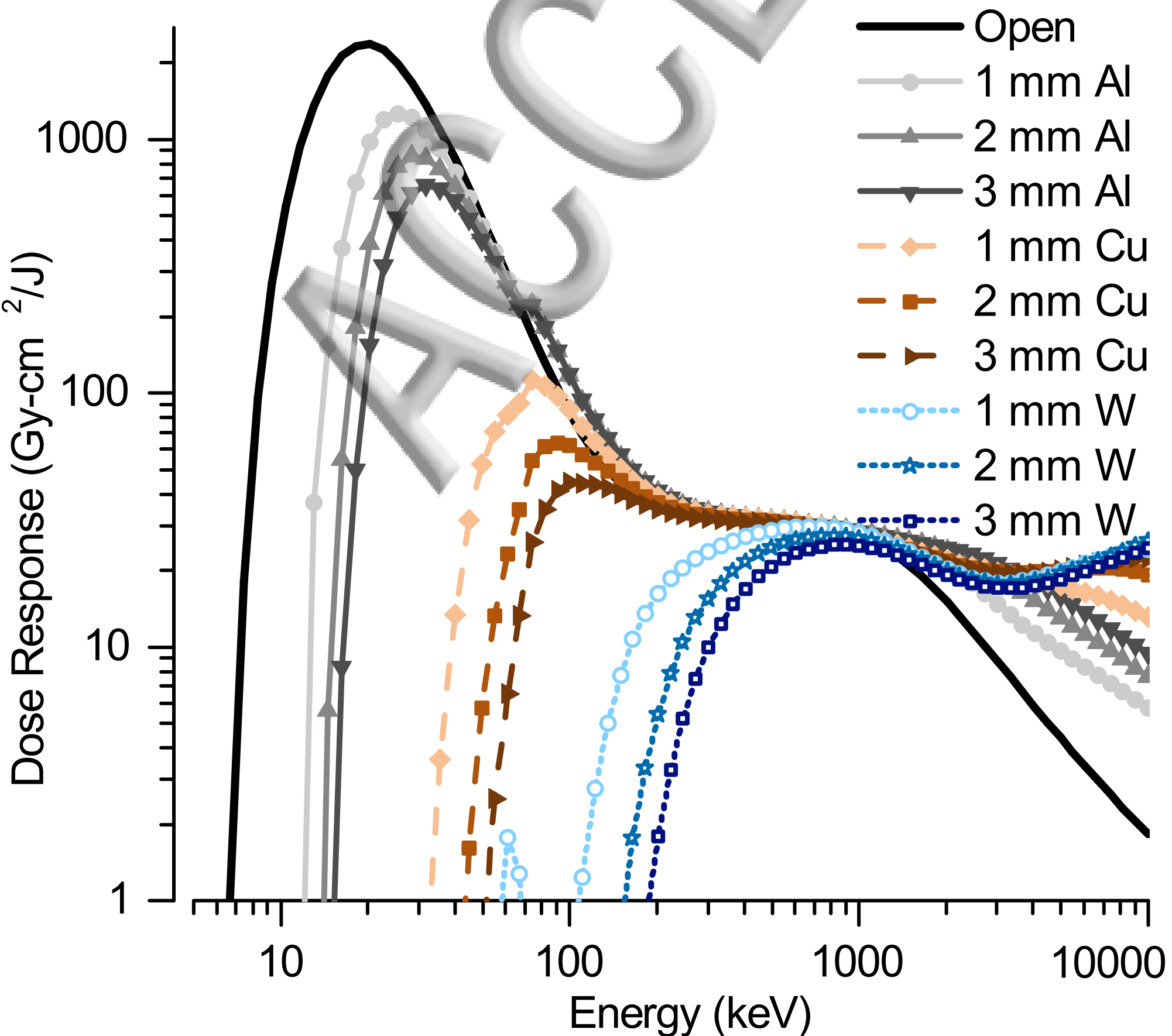
Open
1 mm Al
2 mm Al
3 mm Al
1 mm Cu
2 mm Cu
3 mm Cu
1 mm W
2 mm W
3 mm W
1000
100
10
1
Dose Response (Gy-cm 2/J)
10
100
1000
10000
Energy (keV)

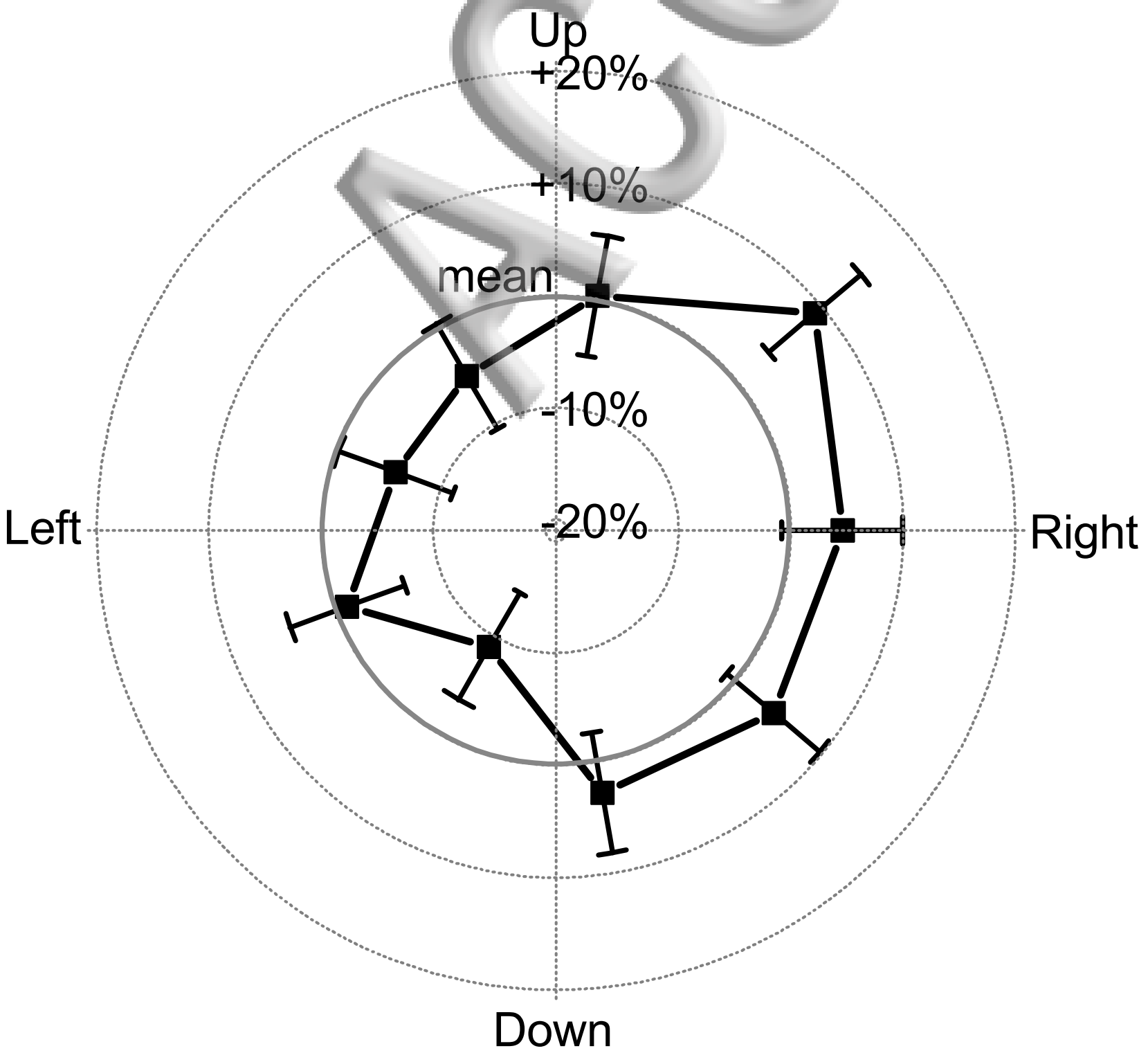
Up
+20%
+10%
mean
-10%
-20%
Left
Right
Down

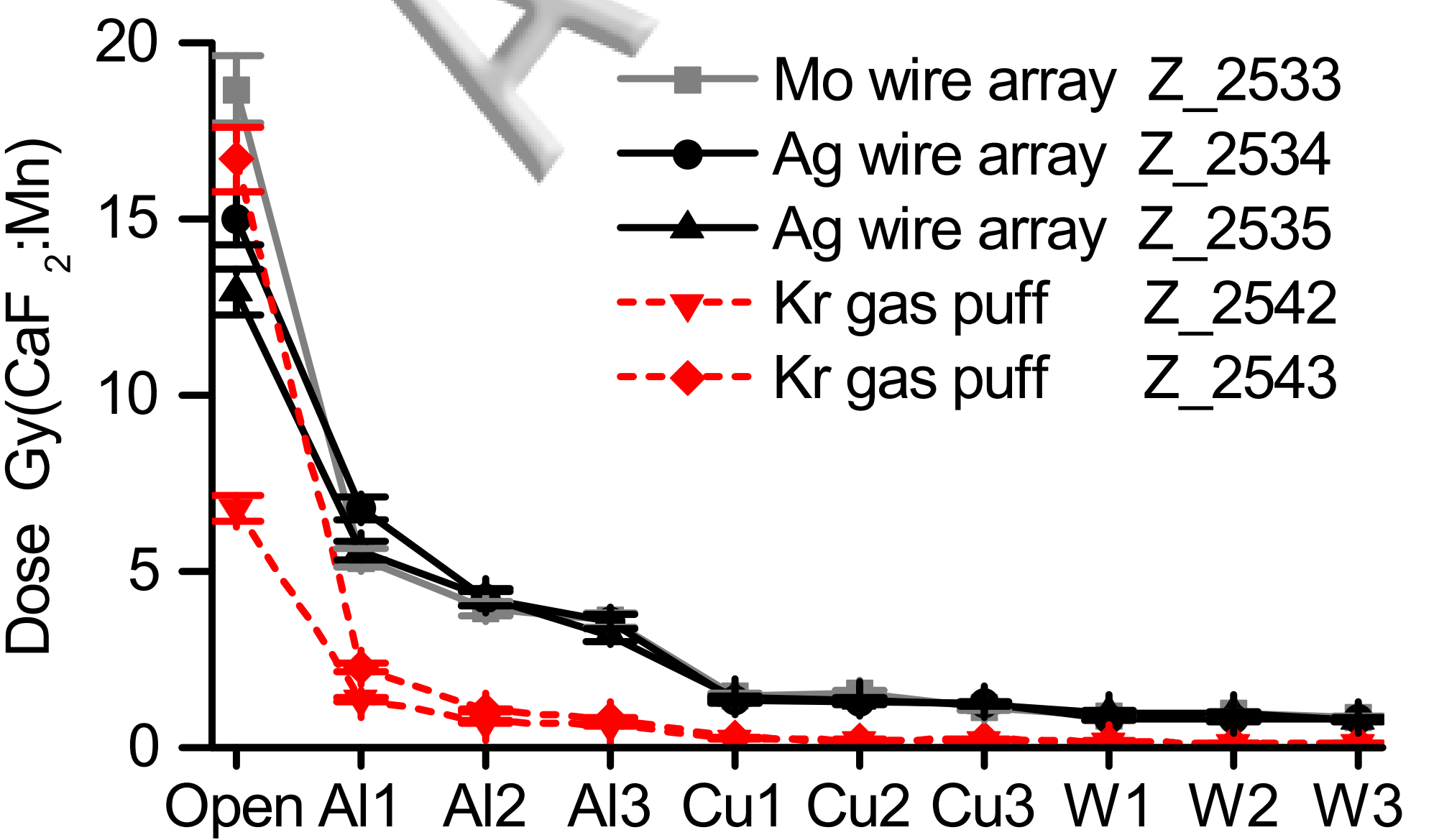
Dose Gy(CaF2:Mn)
20
15
10
5
0
Open
Al1
Al2
Al3
Cu1
Cu2
Cu3
W1
W2
W3
Mo wire array Z_2533
Ag wire array Z_2534
Ag wire array Z_2535
Kr gas puff Z_2542
Kr gas puff Z_2543

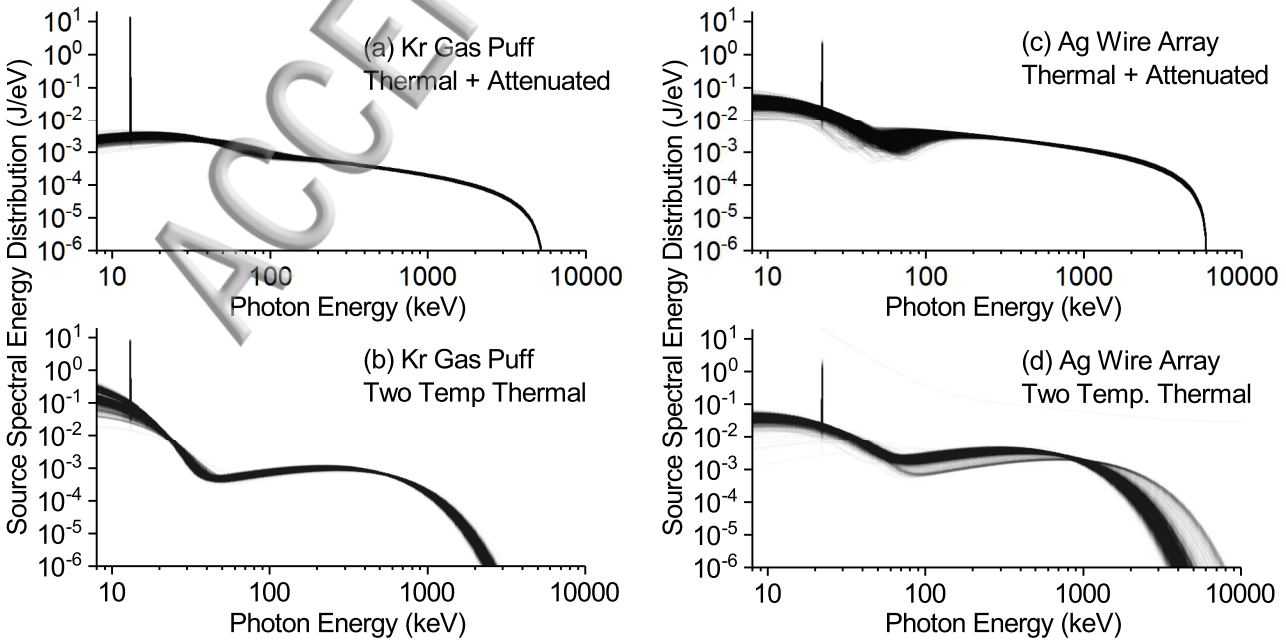
(a) Kr Gas Puff
Thermal + Attenuated
(b) Kr Gas Puff
Two Temp Thermal
(c) Ag Wire Array
Thermal + Attenuated
(d) Ag Wire Array
Two Temp. Thermal
Source Spectral Energy Distribution (J/eV)
Photon Energy (keV)
10
100
1000
10000
10^{1}
10^{0}
10^{-1}
10^{-2}
10^{-3}
10^{-4}
10^{-5}
10^{-6}

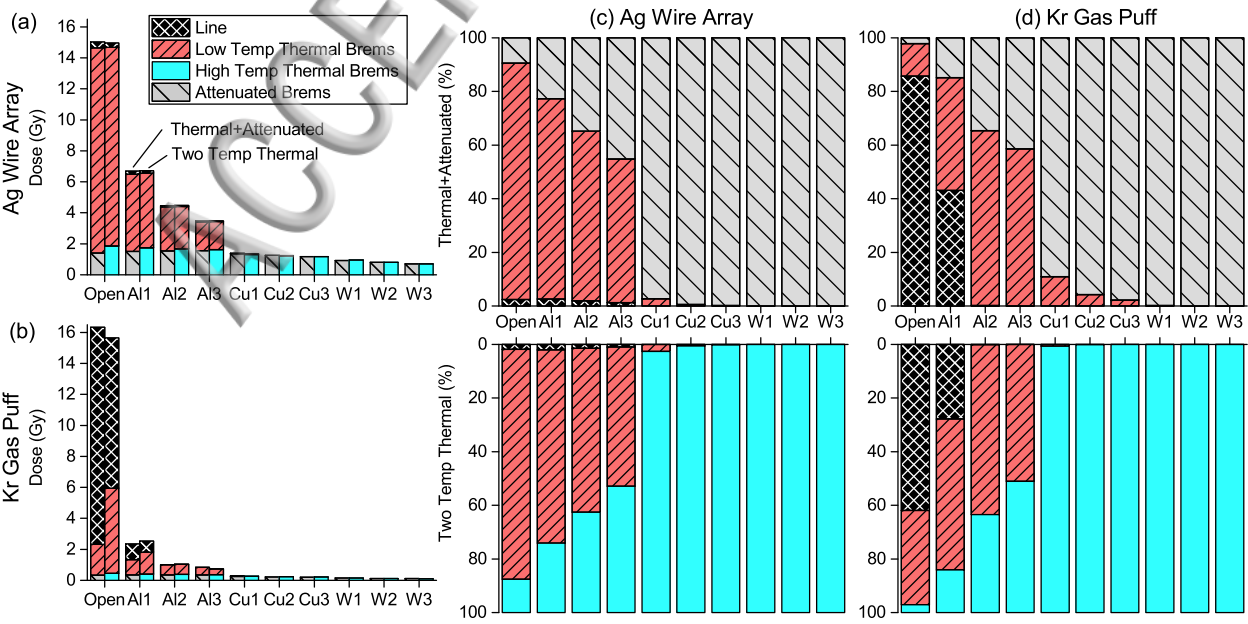
(a)
Ag Wire Array
Dose (Gy)
Line
Low Temp Thermal Brems
High Temp Thermal Brems
Attenuated Brems
Thermal+Attenuated
Two Temp Thermal
Open Al1 Al2 Al3 Cu1 Cu2 Cu3 W1 W2 W3
(b)
Kr Gas Puff
Dose (Gy)
(c) Ag Wire Array
(d) Kr Gas Puff
Thermal+Attenuated (%)
Two Temp Thermal (%)

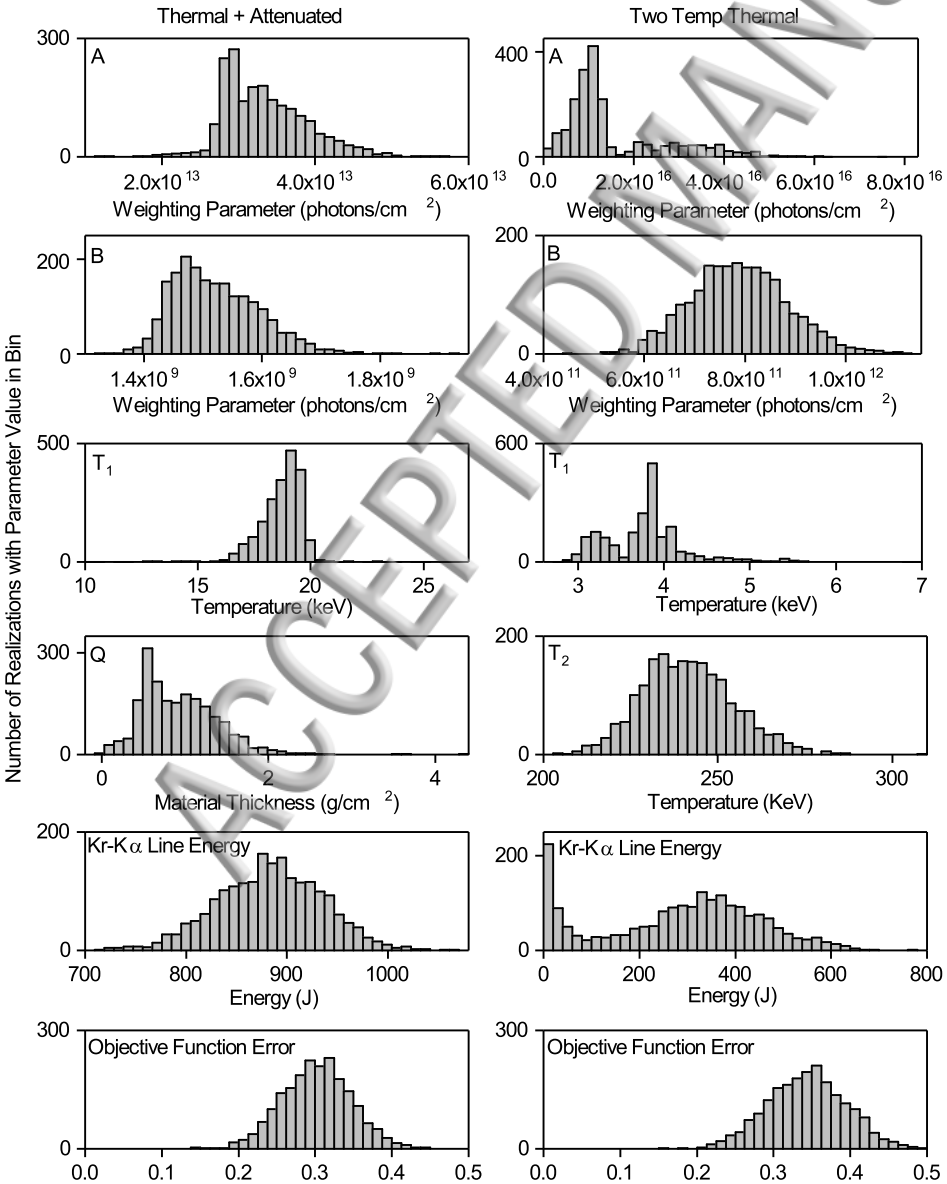
Thermal + Attenuated
Two Temp Thermal
A
B
T_1
Q
T_2
Kr-Kα Line Energy
Objective Function Error
Number of Realizations with Parameter Value in Bin
Weighting Parameter (photons/cm ^{2})
Temperature (keV)
Material Thickness (g/cm ^{2})
Temperature (KeV)
Energy (J)
ACCEPTED MANUSCRIPT

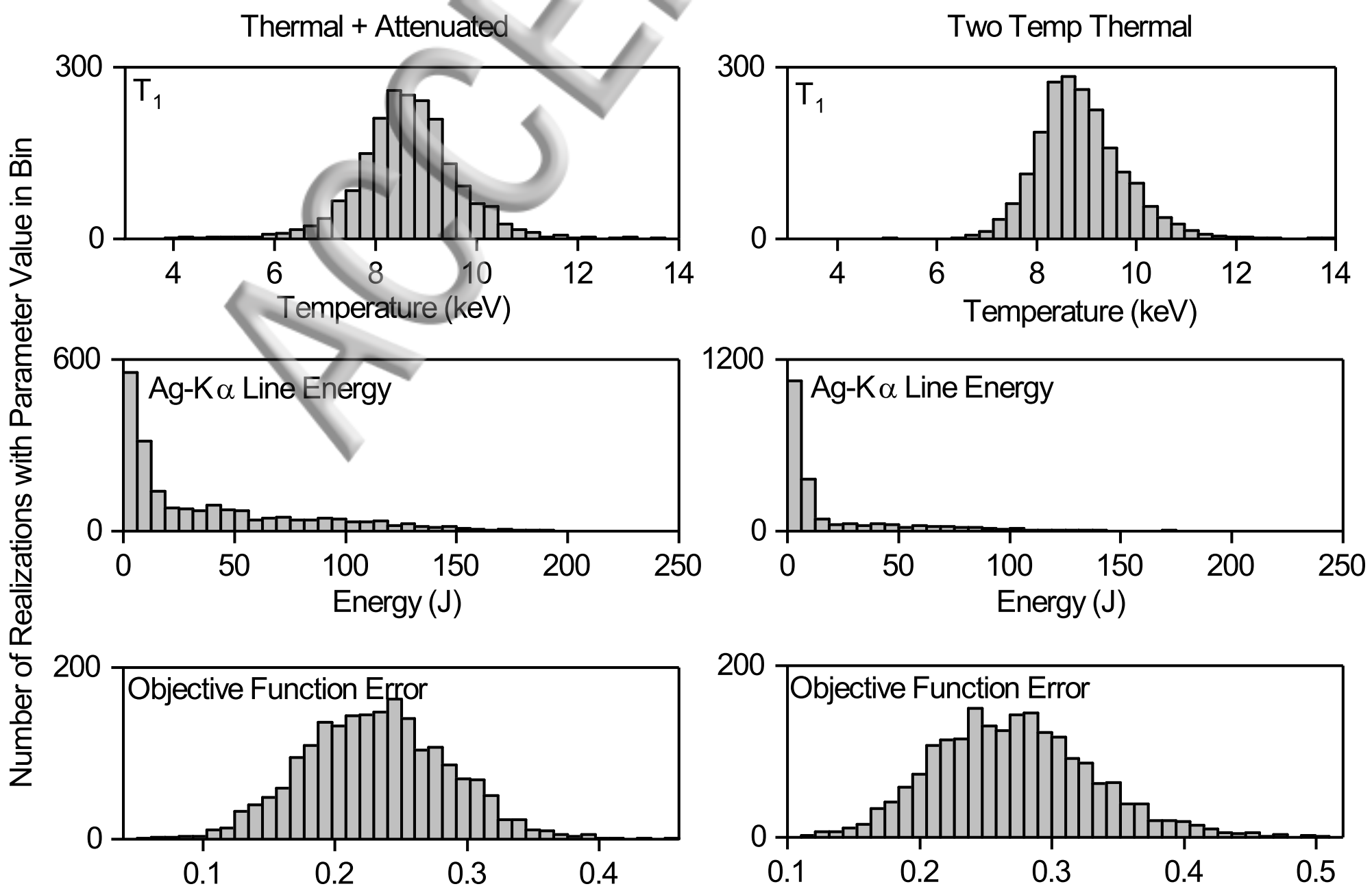
Thermal + Attenuated
Two Temp Thermal
Number of Realizations with Parameter Value in Bin
300
0
T1
4
6
8
10
12
14
Temperature (keV)
600
1200
Ag-Kα Line Energy
0
50
100
150
200
250
Energy (J)
200
Objective Function Error
0.1
0.2
0.3
0.4
0.5

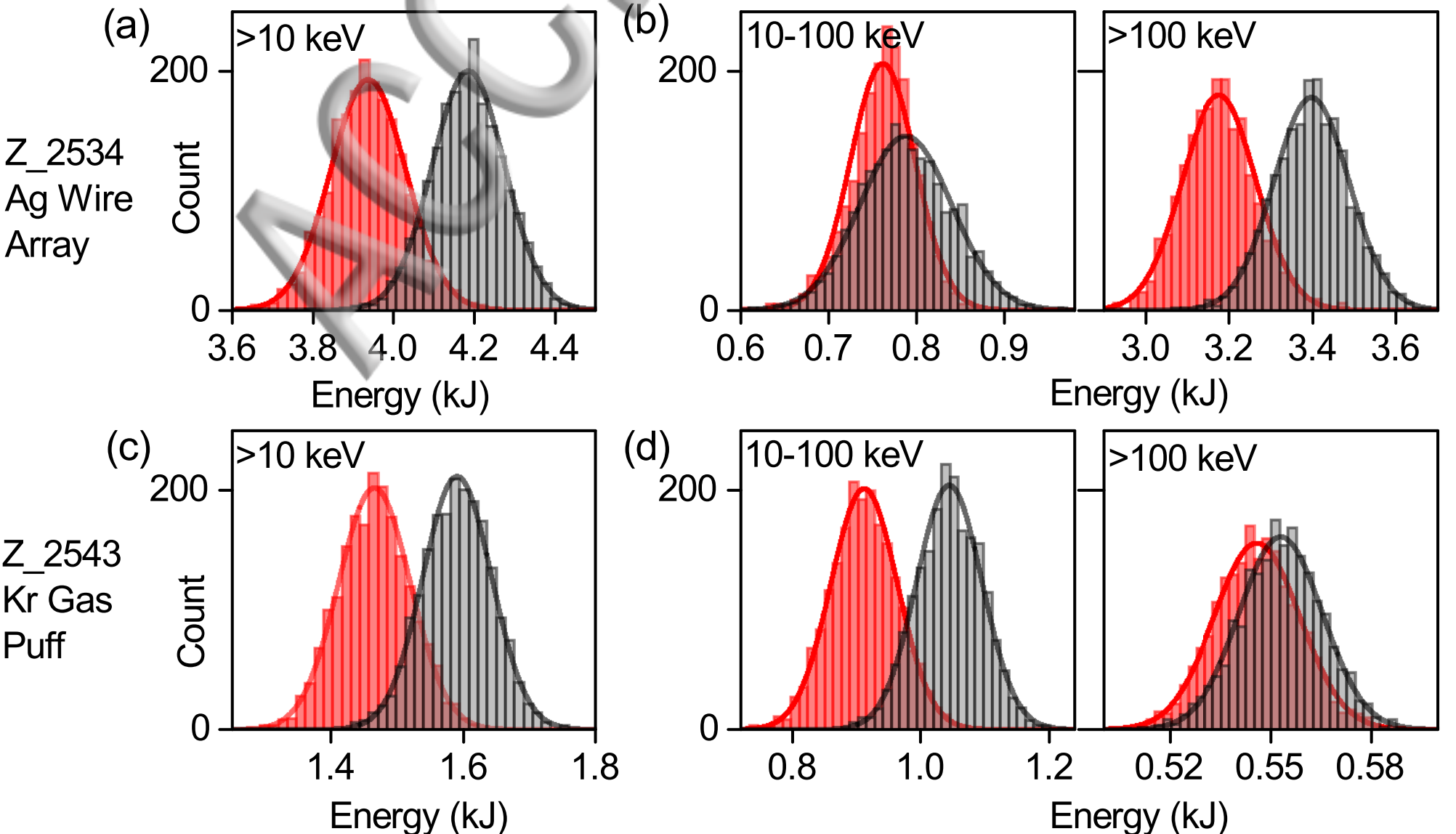
(a)
>10 keV
200
0
Count
3.6
3.8
4.0
4.2
4.4
Energy (kJ)
(b)
10-100 keV
>100 keV
200
0
0.6
0.7
0.8
0.9
3.0
3.2
3.4
3.6
Energy (kJ)
Z_2534
Ag Wire
Array
(c)
>10 keV
200
0
Count
1.4
1.6
1.8
Energy (kJ)
(d)
10-100 keV
>100 keV
200
0
0.8
1.0
1.2
0.52
0.55
0.58
Energy (kJ)
Z_2543
Kr Gas
Puff